Computation of Electromagnetic Field and Complex Materials Interaction

R. S. Qin[1,2]

[1]School of Engineering & Innovation, The Open University, Walton Hall, Milton Keynes MK7 6AA, UK
[2]Department of Materials, Imperial College London, Exhibition road, London SW7 2AZ, UK

Abstract— We develop a method to calculate the electromagnetic field distribution in complex materials. The system contains multiple phases with different electrical and magnetic properties and also contains multiple components which can diffuse around to affect the local electromagnetic properties. Based on the calculations we are able to determine the interaction between electromagnetic field and materials microstructure and property evolutions. It is possible to use electromagnetic field to drive materials phase and compositions to redistribute. Using the theoretical predictions we have made many novel materials which are not possible to achieve by other conventional method. It is possible to use electromagnetic field to manipulate nano-scale gas bubbles, liquid droplets and solid inclusions in materials matrix.

1. INTRODUCTION

A complex material consists of multiple phases and multiple components [1]. Different phases and a phase with different compositions have different electrical (e.g. electrical conductivity, dielectric coefficient, etc) and/or magnetic (e.g. magnetic permeability) properties [2, 3, 4, 5]. The configuration of the phases and components is called materials microstructure. An electric field, magnetic field or electromagnetic field can be affected by the materials microstructure [6]. Solving the distribution of electromagnetic field inside and outside the complex materials has been the research focus in electromagnetic kinetics for long history. What more important but less focused is the electromagnetic field could be used to change the materials microstructure [7, 8]. This is called the interaction between electromagnetic field and the complex materials.

This work will introduce our efforts in investigation of the electromagnetic field and complex materials interaction. The electric and magnetic properties of each phase with knowing chemical constitution and environment parameters (temperature and pressure) can be measured easily by experimental facilities. The initial microstructure of a complex material can be obtained by various microscopes. The configuration of electromagnetic field can be obtained by solving Maxwell?s equations under various boundary conditions. This leads to the thermodynamic property of electromagnetic field associated free energy. The second law of thermodynamics predicts the materials microstructure evolution in order to reduce the free energy into minimum. By which we are able to predict the adjustment of materials microstructure and associated electromagnetic field redistribution. The iteration reveals the total trajectory of electromagnetic field and complex materials interaction. One thing to be pointed out is that the interaction is beyond the traditional concepts of electrophoresis, magnetophoresis and electromagnetophoresis.

2. THEORETICAL CONSIDERATION

One starts with a consideration of electric field and electric neutral nonmetallic inclusion interaction in conductive liquid. The electric field free energy of a material carrying electric current is associated with the current density distribution. The configuration that possesses the lowest system free energy is thermodynamically preferred. An inclusion intends to move from one position having high system free energy to another having low system free energy. This is equivalent to the existence of a driving force that transports the inclusion from a high free energy location to the low free energy location. The question is how strong the force is and what the properties of the force are. According to Ohm?s law, the local electric current density is determined by the local electrical conductivity and the local electric field, i.e. $\vec{j}(r) = \sigma(r) \cdot \vec{E}(r)$, where r is a spatial position in material, $\vec{j}(r)$ the local electric current density, $\sigma(r)$ the local electrical conductivity and $\vec{E}(r)$ the local electric field. The electric field is determined by the gradient of the local electric potential by $\vec{E}(r) = -\nabla\phi(r)$, where $\phi(r)$ is the local electrical potential. Gauss's law represents the relationship between the

local electric field and the local electric charge density as $\nabla \cdot \vec{E}(r) = \rho(r)/\epsilon_0$, where $\rho(r)$ is the local charge density and ϵ_0 the permeability of free space. For a metallic matrix containing electrically neutral inclusions, nowhere in the material has net charge. This enables Gauss's law to reduce to Poission?s equation, as expresses in followings

$$\nabla^2 \phi(r) = 0 \tag{1}$$

The distribution of the electric potential in the system consisting of metal matrix and the electrically neutral inclusions can be obtained by solving Eq.1 with adequate boundary conditions. The analytical solution has been worked out for a few systems having high symmetrical boundary geometries, e.g. a spherical or cylindrical inclusion in an infinity large matrix [9, 10]. The solution for more complicated boundary conditions can be obtained by discrete numerical calculation. Eq. 1 can also be represented as $\nabla \cdot \vec{j}(r) = 0$. This is equivalent to the statement of Kirchhoff's current law and can be used as the governing equation for calculating the distribution of electric potential and the distribution of electric current density using relaxation method. The resolved distribution of electric current density can be used to calculate the system free energy associated with the electric current by [6].

$$G_j = \frac{1}{8\pi} \iint_V \frac{\mu \vec{j}(r) \cdot \vec{j}(r')}{|r - r'|} dr dr' + G_{ref} \tag{2}$$

where G_j is the system free energy associated with electric current, μ the magnetic permeability, V the volume of material and G_{ref} the system free energy at the reference state, respectively. When an inclusion is relocated from position d to $d + \Delta d$ which causes the system free energy changes from $G_j(d)$ to $G_j(d + \Delta d)$, the equivalent driving force from the electric current to the inclusion is expressed as

$$\vec{F}(d) = -\frac{\delta G_j(d)}{\delta d} = -\lim_{\Delta d \to 0} \frac{G_j(d + \delta d) - G_j(d)}{\Delta d} \tag{3}$$

The force from the electric current to electrically neutral inclusion is non-zero if the effect of the reconfiguration of an inclusion on the redistribution of the electric current density is not negligible.

3. NUMERICAL CALCULATION AND RESULTS

Numerical calculations have been performed to a piece of rectangular metal subjected to 20 volts electric potential differences (Fig. 1, A). The dimensions of the sample are measured as 10 cm long, 2 cm wide and 0.2 cm thick, which are the typical sizes of samples used in electropulsing experiments [11]. The electrical conductivity of the metal matrix is assumed to be $\sigma_m = 1.0 \times 10^7 \Omega^{-1} \cdot m^{-1}$, which is equivalent to the resistivity of pure iron at room temperature. The electrical resistance of the sample without inclusion is $2.5 \times 10^{-4} \Omega$. The average electric current density is $2.0 \times 10^9 A \cdot m^{-2}$, which is in the same order as that used in many electropulsing processing experiments [12, 13] but is at least 3 orders of magnitude smaller than the current-induced magnetization switching [14]. An electrically neutral inclusion with radius r_i and electrical conductivity $\sigma_i = \eta \sigma_m$ is embedded in the metal matrix with its centre in the distance from the centre of the matrix vertically (Fig. 1, A), where η is the ratio between the electrical conductivity of inclusions and that of matrix. In the present work, one has $0 < \eta < 1$ because the electrical conductivity of inclusion is smaller than that of metal matrix. The magnetic permeability of matrix is supposed to be the same as that of inclusion, which is assumed the same as that of vacuum and has $\mu = 1.2566 \times 10^{-6} H \cdot m^{-1}$.

In the discrete computation, the geometry of inclusion is represented using the staircase approximation. A lattice is either located inside the inclusion or the matrix. Two neighbouring lattices are linked by an element. The electrical conductivity of the element has $\sigma_e = \sigma_i$ when both lattices at two ends of the element are inside the inclusion, $\sigma_e = \sigma_m$ when both lattices are inside the matrix, or $\sigma_e = 2\sigma_m \sigma_i / (\sigma_m + \sigma_i)$ when one of the lattices is located inside the inclusion and another inside the matrix. The distribution of the electric current density is calculated using the relaxation method and then substituted into Eq. (2) to calculate $G_j(d)$. For convenience $G_j(0)$ is defined as the reference, where $d = 0$ implies that the inclusion is located at the centre of the matrix. The numerical results for an inclusion whose radius is 0.08 cm and conductivity ratio in various values reveal that $G_j(d)$ at $d = 0$ has the largest value (Fig. 1, B). $G_j(d)$ decreases monotonically when d increases until the most distant surface of the inclusion is near to the surface of the matrix (labelled

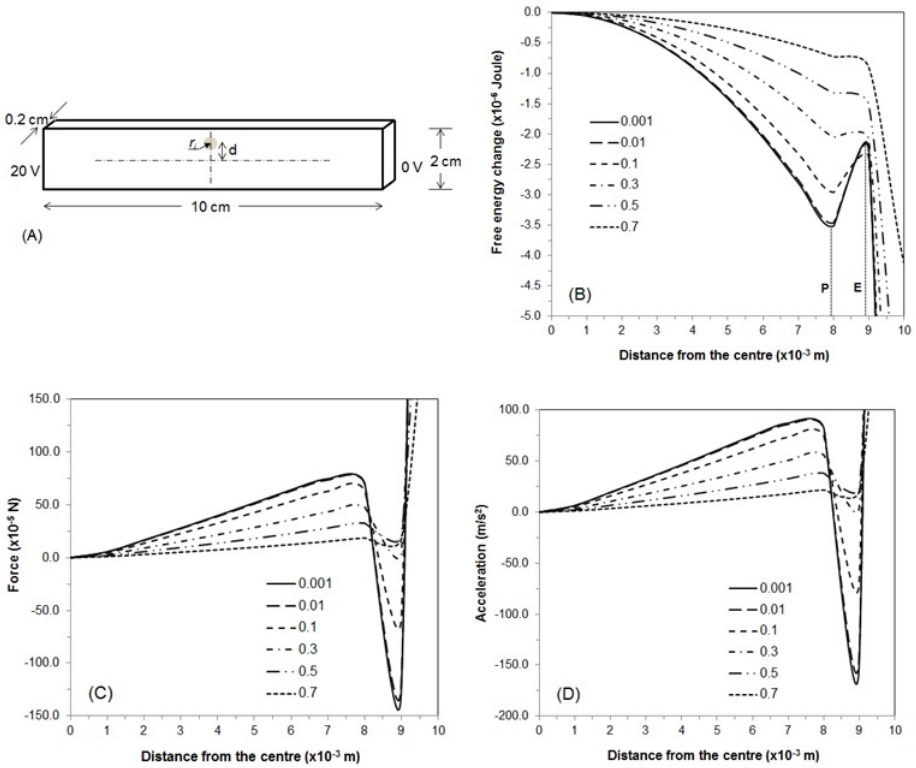

Figure 1: The numerical calculations for the effect of electric current on an electrically neutral inclusion in metal matrix. (A) The system dimensions and the setup of electric potentials. (B) The change of system free energy vs. the distance from the centre of the metal matrix to the centre of inclusion at various conductivity ratios. (C) The equivalent force vs. the position of the inclusions at various conductivity ratios. (D) The acceleration of generated by the force to a MnS inclusion vs. the position of the inclusion at various assumed conductivity ratios.

by position P in Fig. 1, B). Beyond this point, $G_j(d)$ increases anomalously as the increasing of d until the most distant surface of the inclusion touches the surface of the matrix (labelled by position E in Fig. 1, B). Despite the anomalous increasing, $G_j(0)$ is always the highest system free energy. Beyond the position E, the inclusion moves away from the matrix and $G_j(d)$ decreases sharply as the increasing of d until the inclusion is detached from the matrix completely. The change of $G_j(d)$ as the increasing of d is more severe when $\eta = \sigma_i/\sigma_m$ is smaller (Fig. 1, B). However, the differences are indistinguishable when $\eta < 0.01$. The force from the electric current to an electrically neutral inclusion in the case has been calculated using Eq. (3) (Fig. 1, C). The positive force at $0 < d < P$ means the electric current intends to move an inclusion from the centre of the matrix toward the surface. The area can be called pushing zone. The force is negative in the area with $P < d < E$. An inclusion will be trapped into the area around P. The free energy achieves a local minimum (Fig. 1, B) and the force achieves zero at position P (Fig. 1, C). The area with $P < d < E$ can be called a trapping zone. The force becomes a strong positive value at $d > E$ and the inclusion will be expelled out of the matrix. This area can be called an expelling zone. Electric current helps to remove inclusion from matrix at this area and prevent any inclusion from coming into the metal matrix. To demonstrate the strength of the force from the electric current to the electrically neutral inclusion, the inclusion is assumed to have a density of $3990kg \cdot m^{-3}$, which is the density of MnS particle at room temperature. The acceleration caused by the force to the inclusion particle has been calculated (Fig. 1, D). For the parameters $r_i = 0.08cm$ and $\eta = 0.01$, the acceleration at $d = 0.1cm$ is $6.32m/s^2$ and at $d = 0.2cm$ is $19.06m/s^2$. The latter is greater than the gravitational acceleration. The majority of the other points on the curve with $\eta = 0.01$ have acceleration greater significantly than the gravitational accelerations.

Further numerical calculations have been done to characterize the properties of the force (F) generated by the electric current to the inclusion. Firstly, one defines $\xi = (\sigma_m - \sigma_i)/(2\sigma_m + 2\sigma_i) = (1-\eta)/(2+\eta)$ and plots the relationship between F/ξ and d for various values of η (Fig. 2, A). All the lines at the pushing zone ($0 < d < P$) are close to each other although there are significant

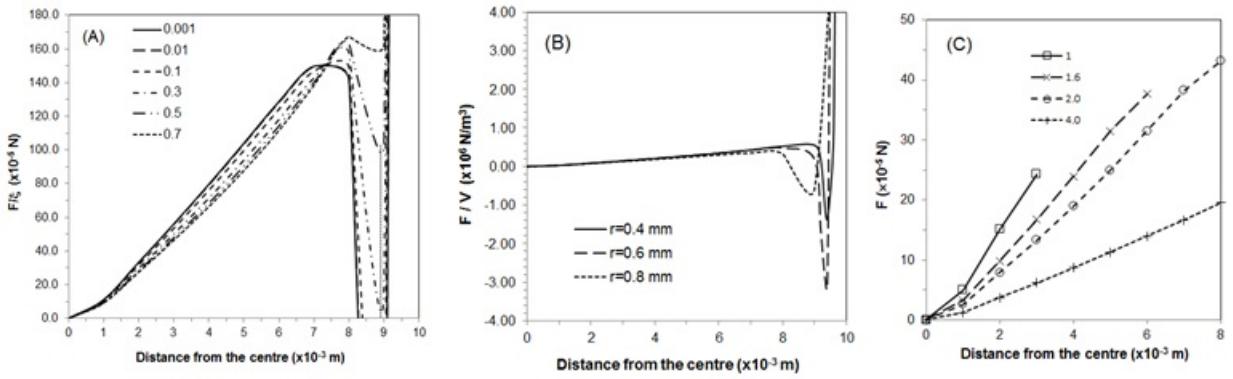

Figure 2: The properties of the force. (A). The force divided by $\xi = (1-\eta)/(2+\eta)$ as a function of the distance from the centre of the matrix to the centre of the inclusion for various values of η. (B). The force divided by the volume of the inclusion as a function of inclusion?s location for inclusions with different radiuses. (C). The variation of force as a function of inclusion?s location for the matrix with different widths.

differences in the trapping zone and expelling zone. In a rough approximation, one can say that the force is proportional to the factor ξ in the pushing zone. Secondly, numerical calculations for the inclusions whose radiuses are 0.04 cm, 0.06 cm and 0.08 cm at $\eta = 0.01$ have been performed (Fig. 2, B). The lines for the relationships between F/V_i and d fall into the same line in pushing zone ($0 < d < P$), where V_i is the volume of the inclusion. This suggests that the force is proportional to the volume of inclusion in the pushing zone. Thirdly, the relationship between F and d has been calculated when the width of the sample is changed from 2 cm to 1 cm, 1.6 cm and 4.0 cm, respectively (Fig. 2, C). It can be considered approximately that F is proportional to d for various width of the matrix. The slope of the line is dependent on the width of the matrix. The smaller width of the sample has the steeper slope of the line representing F vs. d relationship. In summary, one can represent the force at pushing zone as the following format

$$F = \mu j_0^2 \frac{d}{f(d)} \frac{\sigma_m - \sigma_i}{2\sigma_m + \sigma_i} V_i = \mu j_0^2 \frac{d}{f(d)} \frac{1-\eta}{2+\eta} \tag{4}$$

where $f(d)$ increases monotonically as d increases. The width of the sample is usually much larger than that of the size of inclusion. The pushing zone is, therefore, the dominant area across the matrix.

The differences between the force revealed in the present work and that in the electromagnetophoresis are followings. (1) The direction of the force in electromagnetophoresis is in a fixed direction perpendicular to both the magnetic field and the electric current for $\eta < 1$. While the force in the present work is not in a fixed direction but is from the centre of the matrix to the lateral surface for $\eta < 1$. The latter is axial symmetrical but the former is not. (2) The amplitude of the force in electromagnetophoresis is not location dependent. While the force revealed in the present work is location dependent. (3) There are three different zones for the force revealed in the present work, namely the pushing zone, the trapping zone and the expelling zone. There are no such zones reported for the force in electromagnetophoresis. (4) The force revealed in the present work does not require any external magnetic force, while the force in electromagnetophoresis requires an external magnetic field in addition of the electric current.

From Eq. 4, one predicts that the electric current can be used to drive inclusions in liquid metal to move toward the surface. Experiments have been carried out to validate this prediction. The experimental procedure is similar to that reported in reference [15]. A piece of steel containing MnS inclusions has been molten in a graphite crucible. A pair of iron bars is submerged into the liquid steel to act as the electrodes for conducting electric current. The temperature of the liquid steel is lower than the melting temperature of iron bar. To compare the microstructures of the samples with and without electric current treatment, one set of liquid was solidification without electric current treatment but with exactly the same thermal treatment history, even the electrodes were submerged in the liquid without connecting the power. Another set of sample was treated with the electric current. To prevent the ohm?s heat, electric current pulses have been applied. The pulse is in square wave to reduce the skin effect. Each pulse has a loading duration of $60\mu s$,

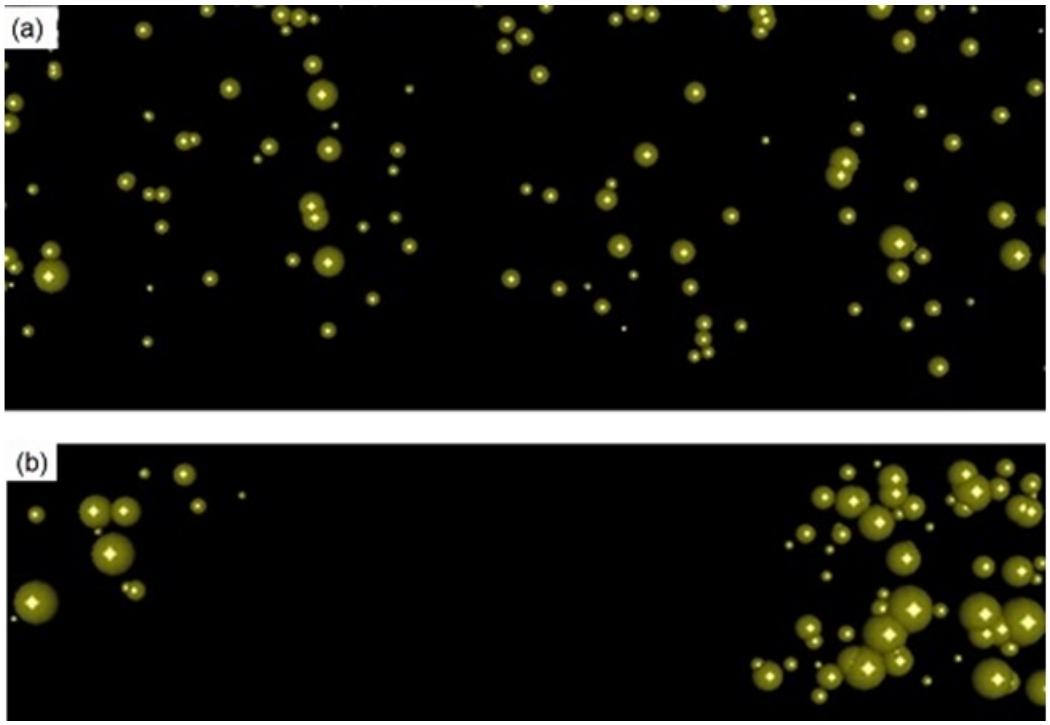

Figure 3: The experimental observed effect of electric current on the reconfiguration of inclusions. (a) without electric field; (b) with electric field.

current density of $1.6 \times 10^6 A/m^2$. The total treatment time is 10 minutes. The frequency of the pulse during the treatment was 1 Hz. The sample is in a width of 2.2 cm. An optical microscope has been used to examine the distribution of the inclusions across the sample. It has been noticed that the number of inclusions in each optical image is distributed almost uniformly in the sample without electric current treatment, but is in a vertical double well form in the sample treated by electric current (Fig. 3). The inclusions in the middle area of the sample are almost pushed away by the electric current. In the area close to the surface, the number of inclusions achieves local maximum. This shows the trapping effect of electric current to the inclusion at the zone. Further toward the surface, the number of inclusions is reduced. This shows the effect of expelling from the current to the inclusions. The experiments have been repeated for a number of times and the similar results are confirmed.

4. CONCLUSION

We have proved that it is not only that the distribution of electromagnetic field is affected by the complex microstructure of materials. The microstructure can also been affected significaly by the applied electromagnetic field. With careful designed external electromagnetic field setting, novel materials and a materials with novel functionality can be produced by using the electromagnetic and materials microstructure interaction.

ACKNOWLEDGMENT

The work was financially supported by EPSRC (EP/L00030X/1) and the Royal Society Newton Advanced Fellowship (NA150320).

REFERENCES

1. Qin, R. S., Wallach, E. R. and Thomson, R. C., "A phase-field model for the solidification of multicomponent and multiphase alloys," *J. Cryst. Growth.*, Vol. 279, 163–169, 2005.
2. Bohnenkamp, U, Sandstrm, R and Grimvall, G, "Electrical resistivity of steels and face-centered-cubic iron," *J. Appl. Phys*, Vol. 92, 4402–4407, 2002.
3. Zhang, P., Wang, X. B., Wang, W., Lei, X. and Yang H., "Iron carbide and nitride via a flexible route: synthesis, structure and magnetic properties," *RSC Adv.*, Vol. 5, 21670–21674, 2015.

4. Thompson, S. M. and Tanner, B. K., "The magnetic-properties of pearlitic steels as a function of carbon content," *J. Magn. Magn. Mater.*, Vol. 123, 283–298, 1993.
5. Hao, X. J., Yin, W., Strangwood, M., Peyton, A.J., Morris, P.F. and Davis, C.L., "Off-line measurement of decarburization of steels using a multifrequency electromagnetic sensor," *Scr. Mater.*, Vol. 58, 1033–1036, 2008.
6. Qin, R. S. and Bhowmik, A., "Computational thermodynamics in electric current metallurgy," *Mater. Sci. Technol.*, Vol. 31, 1560–1563, 2015.
7. Qin, R. S., Rahnama, A. Lu, W. J., Zhang, X. F. and Elliott-Bowman, B., "Electropulsed steels," *Mater. Sci. Technol.*, Vol. 30, 1040–1044, 2014.
8. Qin, Rongshan, "Using electric current to surpass the microstructure breakup limit," *Sci. Rep.*, Vol. 7, 41451, 2017.
9. Kolin, A., "An electromagnetokinetic phenomenon involving migration of neutral particles," *Science*, Vol. 117, 134–137, 1953.
10. Leenov, D. and Kolin, A., "Theory of electromagnetophoresis. I. Magnetohydrodynamic forces experienced by spherical and symmetrically oriented cylindrical particles," *J. Chem. Phys.*, Vol. 22, 683–688, 1954.
11. Qin, R. S., Samuel, E. I. and Bhowmik, A., "Electropulse-induced cementite nanoparticle formation in deformed pearlitic steels," *J. Mater. Sci*, Vol. 46, 2838–2842, 2011.
12. Lu, W. J. and Qin, R. S., "Stability of martensite with pulsed electric current in dual-phase steels," *Mater. Sci. Eng. A* , Vol. 677, 252–258, 2016.
13. Lu, W. J. and Qin, R. S., "Influence of kappa-carbide interface structure on the formability of lightweight steels," *Mater. Des.* , Vol. 104, 211–216, 2016.
14. Krause, S., Berbil-Bautista, L., Herzog, G., Bode, M. and Wiesendanger, R. "Current-induced magnetization switching with a spin-polarized scanning tunneling microscope ," *Science* , Vol. 317, 1537–1540, 2007.
15. Zhang, X. F. and Qin, R. S., "Controlled motion of electrically neutral microparticles by pulsed direct current," *Sci Rep*, Vol. 5, 10162, 2015.